Astron. Astrophys. 267, 559–565 (1993)

ASTRONOMY AND ASTROPHYSICS

A kinematical study of the jet GGD 34*

Ana I. Gómez de Castro [1], L. F. Miranda [2], and C. Eiroa [3]

[1] ESA IUE Observatory**, P.O. Box 50727, E-28080 Madrid, Spain
[2] Departamento de Astrofísica, Universidad Complutense de Madrid, E-28040 Madrid, Spain
[3] Departamento de Física Teórica, C-XI, Facultad de Ciencias, Universidad Autónoma de Madrid, E-28049 Madrid, Spain

Received April 28, accepted July 26, 1992

Abstract. CCD images and spectra of high spectral resolution of GGD 34 are analyzed. The object is a jet consisting of three major condensations separated 0.08 pc one of each other and aligned over 0.17 pc in the east-west direction. The three condensations emit strongly in [S II], [N II] and Hα. The westernmost condensation has also significant continuum emission coming from what seems to be the bow-shaped borders of a cavity. A detailed study of the excitation conditions, densities and velocity field is presented. The excitation of the object is very low and the line ratios can be reproduced by mild radiative shocks at velocities $\leqq 40\,\mathrm{km\,s^{-1}}$. The radial velocity of the gas is high, $\simeq 180\,\mathrm{km\,s^{-1}}$, indicating that the excitation is much lower than expected if the flow kinetic energy is fully spent into gas heating. This is generally observed in young stellar objects (YSO) jets. The exciting source of the outflow seems to be located at the western end of GGD 34, illuminating the cavity.

The two easternmost condensations GGD 34/B and GGD 34/C are connected by a neatly shaped lobe emitting in [S II] and Hα. The width of the lobe varies from 0.012 pc in the condensations to 0.034 in the space in between. The lobe is not symmetric with respect to the jet axis but has a rather sinusoidal morphology. The velocity field in this region also can be well fitted by a sine curve. Morphology and velocity field are correlated; however they are not accompanied by significant changes in the excitation degree. We suggest that the properties of GGD 34 are produced by a "kink" plasma instability.

Key words: interstellar medium: individual objects: GGD 34 – interstellar medium: jets and outflows – stars: pre-main-sequence – instabilities

1. Introduction

Young stellar objects (YSOs) are characterized by very energetic, and often highly collimated mass outflows. The interaction of these outflows with the surrounding medium generates shock excited gas that is seen as highly collimated optical jets and Herbig-Haro (HH) nebulosities. This classification is in part morphologic. Optical jets are seen like beams while HH objects are rather amorphous or bow-shaped nebulosities. However, there is also another difference based on the excitation conditions of the gas. The temperatures inferred from the emission lines coming from the HH objects agree well with what is expected if all the kinetic energy of the gas is dumped into heating. However, the thermal energy content of the jets is much lower than their kinetic energy. This has allowed classification as jets, objects like HH 46/47 (Reipurth & Heathcote 1990) or RNO 43 S/43 N (Mundt et al. 1987), whose properties resemble strongly those of the prototypical jets like HH 34 (Reipurth 1986) except for the lack of good collimation. Wiggles are very apparent along HH 46/47 (Reipurth & Heathcote 1990) and HH 110 (Reipurth 1989). RNO 43 S/43 N has been described as a "diffuse and patchy jet" (Mundt et al. 1987).

In fact, recent observations show that when looked with high enough spatial resolution, jets have wiggles or small departures from extrict cylindrical symmetry. A possible explanation is that the jet comes from a precessing star (Raga et al. 1992). Another obvious possibility is the development of jet instabilities. In this paper, we show a detailed study of GGD 34, a very wiggly jet, that might be a prototype for the study of jet instabilities.

GGD 34 is in NGC 7129, a well known region of star formation, located at 1 kpc from the Sun (Racine 1968). The object was classified as an HH by Hartigan & Lada 1985. Later, Ray 1987 realized that GGD 34 is an optical jet on the basis of narrow band images. CCD images of GGD 34 are also shown by Gómez de Castro 1989 and Eiroa et al. 1992 (hereafter GdC and EGdCM). These lower resolution images show that GGD 34 has three major condensations connected by [S II] and Hα emission. The study of the proper motions indicates that the easternmost condensation is moving towards the east (Ray et al. 1990). During 1988 and 1989, we collected the detailed spectroscopic information and the high resolution images that we analyze in this work. In Sect. 2 we describe the observations we have carried out in detail. The spectra are analyzed in Sect. 3. Electronic densities and excitation conditions are estimated and the position-velocity diagrams for the different slit orientations are studied. The main physical parameters of GGD 34 are summarized in Sect. 4. The constraints imposed by the velocity field of the flow to the hydrodynamics of the jet are analyzed in Sect. 5. The characteristics of GGD 34 suggest that it is a jet undergoing a "kink" instability.

Send offprint requests to: A. I. Gómez de Castro

* Based on observations carried out at the Calar Alto Observatory.

** Affiliated to the Astrophysics Division, Space Science Department, ESTEC.

2. Observations

The observations were carried out in July 1988 (imaging) and August 1989 (long-slit spectroscopy) with the 3.5 m telescope of the Calar Alto Observatory (Almería, Spain).

2.1. CCD images

The images have a scale of 0".254 pix^{-1} and the field of view is 260" × 167". The seeing is 1". The detector was an RCA CCD with 15 μm pixel size. We used two narrow band filters centered in Hα and [S II] ($\lambda_0 = 6567$ Å, $\Delta\lambda = 100$ Å and $\lambda_0 = 6730$ Å, $\Delta\lambda = 95$ Å, respectively), and a broad-band *I* filter with $\lambda_0 = 9140$ Å and $\Delta\lambda = 2000$ Å. The exposure times were 1200 seconds for the narrow band images and 900 seconds for the *I* image. The data have been reduced following standard procedures using the NOAO/IRAF package. Isocontours plots of the three images are shown in Fig. 1. The condensations are denoted following GdC and EGdCM.

GGD 34 extends over 0.17 pc in the east-west direction and its width ranges from 0.012 pc (at 3σ level) in the narrowest end of condensation B to 0.034 pc also at 3σ level measured in the wider regions of the object located between B and C.

GGD 34/A is bow shaped in the *I* frame, with a flux minimum just at the head of the bow which splits it into two parts, the northern being more intense and extended. The *I* flux seems to trace the border of a dark cavity. This border is less apparent in the narrow band images, especially in the [S II] frame, where most of the emission is concentrated at the apex of the bow (flux minimum in *I*) and in a jet-like feature departing eastwards towards condensation GGD 34/B. The Hα emission is also strong at the head of the bow. In addition, significant Hα emission is detected from the northern half of the bow.

The [S II] jet-like feature points from GGD 34/A towards B (see Fig. 1). GGD 34/B is more elongated in [S II] than in Hα and has two subcondensations separated 1".7 (1700 AU) in the east-west direction. The brightest coincides with the peak of the Hα emission and has a faint *I* counterpart. The shape of GGD 34/B in Hα is triangular and has an opening angle of 55°. This opening angle is ≃ 40° in [S II] for the same signal level (~ 3–6σ).

From GGD 34/B to GGD 34/C, the object looks like a thick and stretched lobe that opens up in between the condensations and focusses back at these positions. The lobe is more homogeneous and neatly shaped in [S II] than in Hα. In between the two condensations there is a local maximum in Hα and [S II], suggesting some curvature or limb brightening. Close to the peak of GGD 34/C the northern part of the lobe is brighter in Hα, while the southern is more intense in [S II]. A streamer seems to depart from GGD 34/C eastwards, suggesting that the jet might continue further east although invisible at optical wavelengths.

The shape and position of the maxima in GGD 34/C also vary from Hα to [S II]. The peak of GGD 34/C in [S II] is shifted 0".84 (840 AUs) to the south-west respect to Hα. There is a point-like source inside the condensation C in the *I* band. This does not coincide with any of the maxima of GGD 34/C but it is shifted 2".2 (2200 AUs) to the south-west with respect to the Hα peak confirming the previous results (GdC).

The maxima of the condensations C and B and the [S II] peak of GGD 34/A are aligned along position angle (PA) ≃ 79° defining the *axis* of the object. This alignment is remarkable when compared with the overall apparent sinuosity of the object.

There is a noticeable similarity between GGD 34 and HH 46/47 (see Reipurth & Heathcote 1990 for recent high quality images). HH 46/47 consists of two bright knots or condensations, HH 46 and HH 47, connected by a low excitation filament of 72" length. Some ripples are detected along the filament although they are smaller than those observed in GGD 34. The source driving the outflow is very obscured and cannot be seen directly but illuminates the bright, bow-shaped nebula that surrounds HH 46, in a way very similar to that in which the bow-shaped GGD 34/A condensation surrounds the [S II] jet-like feature departing from the apex.

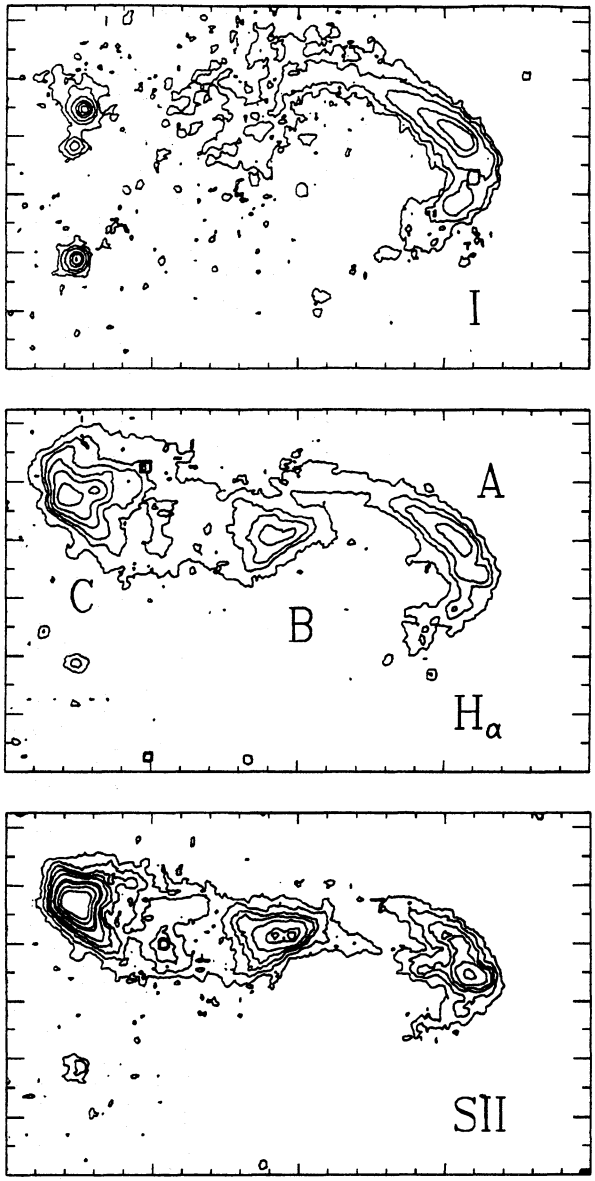

Fig. 1. Isocontours plots of GGD 34 CCD images. Top: *I* band; Middle: Hα; Bottom: [S II]. Isocontours have been selected to enhance the main features. The distance between two tickmarks is ≃ 2".5. North is at the top and east to the left

2.2. Long-slit spectra

Spectroscopy was carried out with the Cassegrain Twin Spectrograph of the 3.5 m telescope. The detector was a GEC CCD with 17 μm pixel size. The scale is 0".634 pix^{-1} and the size of the slit 240". The dispersion is 36 Å mm^{-1} and the slit width 2". The

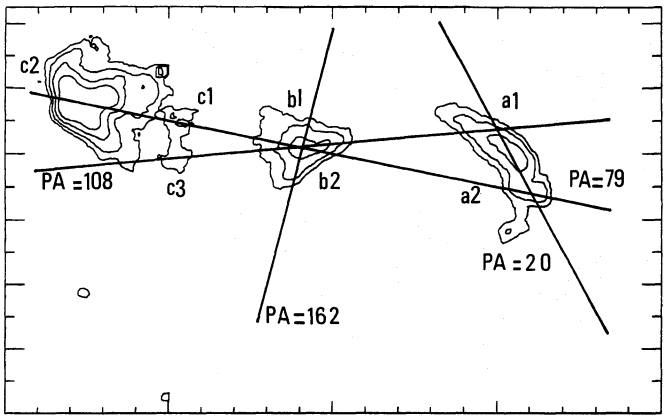

Fig. 2. Orientation of the slits over GGD 34. The main condensations A, B and C are indicated. The locations where the spectra cross each major condensation are also named in the figure. This notation is followed in Figs. 3–5 and in Table 1

effective spectral resolution inferred from the FWHM of the sky lines is 1.86 Å. The spectra cover the range ~6500–6900 Å including the $[N\,II]_{6548,6584}$, $[S\,II]_{6716,6731}$ and Hα lines.

We obtained three spectra with the slit centered in the maximum of the condensation B ($\alpha(1950) = 21^h42^m18^s.5$, $\delta(1950) = 65°54'49''.1$) and PA = +79°, +108° and +162°. The first orientation coincides with the major axis of the object as defined in Sect. 2.1. The second is along the symmetry axis of the condensation B and the third approximately perpendicular to the first orientation (PA = 79°). A fourth spectrum was obtained centered in the [S II] maximum of the condensation GGD 34/A ($\alpha = 21^h42^m15^s.9$, $\delta = 65°54'49''$) and tangent to the bow (PA ≃ 20°). All these slit orientations are shown in Fig. 2 over an isocontour map of the object. The exposure time is 3600 seconds for each spectrum. The data have been reduced following standard procedures and using the NOAO/IRAF package. The 0 of the wavelength scale has been fixed with an accuracy $\leqq 30\,km\,s^{-1}$. The Hα emission associated to the reflection component of GGD 34 is, within the error, at rest with respect to the cloud (NGC 7129) velocity. Also, the velocity inferred from spectra taken with different orientations are coherent among themselves within this accuracy of $30\,km\,s^{-1}$. The spectrum taken with PA = 108° has been shifted by $30\,km\,s^{-1}$ to fit on the others.

The spectra show Hα, [S II] and [N II] emission lines, and a faint continuum associated with GGD 34/A. The relevant lines are plotted in Figs. 3, 4 and 5 for position angles 79°, 108° and 20° respectively. The main knots in each spectrum have been denoted according to Fig. 2.

The first striking feature is the variation of the radial velocity along the major axis of GGD 34 (Fig. 3; PA = 79°). The velocity increases very rapidly in B from west towards east. Three main knots are observed in the path, that correspond to condensation B, the northern part of the lobe and condensation C, respectively. There is a slight decrease in speed from the western end of GGD 34/B towards the center of the condensation, more apparent in Hα than in the other lines. The very rapid increase of the velocity in GGD 34/B is observed in all the lines. Finally the smooth decrease of the velocity close to GGD 34/C also seems to be more intense in Hα.

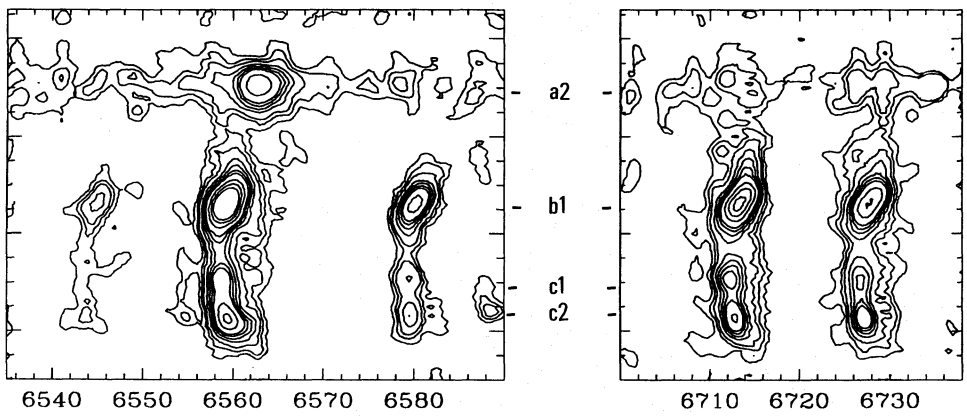

Fig. 3. Isocontours plot of the long-slit spectrum of GGD 34 taken with PA = 79°. Hα and [N II] lines are shown in the left panel and [S II] lines in the right. Wavelength and position along the slit are in the horizontal and vertical axes, respectively. The separation between two tick marks in the vertical direction represents ≃ 3″.2. The condensations "a 2", "b 1", "c 1" and "c 2" correspond to the spatial locations indicated in Fig. 2. West is to the top and east to the bottom

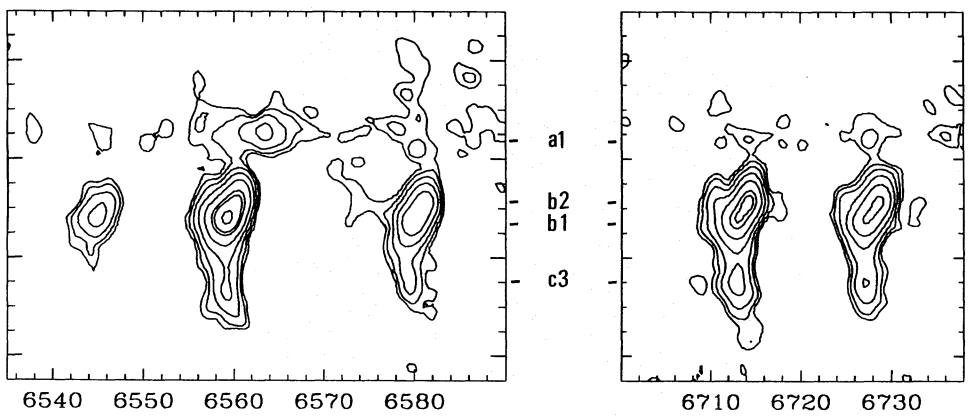

Fig. 4. Idem Fig. 3 for PA = 108°. West is to the top and east to the bottom

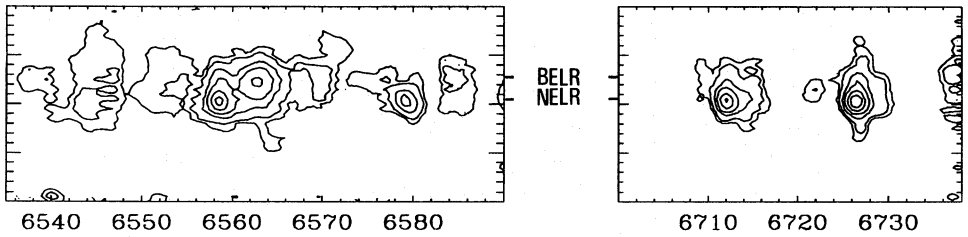

Fig. 5. Idem Fig. 3 for PA = 20°. The separation between two big tick marks in the vertical direction represents ≃ 6″.3. North is at the top and south at the bottom. The NELR and BELR emission is indicated

The condensation A produces a faint continuum and strong Hα emission centered at 0 velocity. The emission is broader in this region than in the rest of the object. There are no bright [S II] lines indicating that the slit does not pass exactly over the very bright [S II] knot observed in the images (see Figs. 1 and 2). Some weak [S II] emission (3σ level) seems to be coming from GGD 34/A.

Figure 4 shows the spectrum of GGD 34 along the major axis of the condensation B (PA ≃ 108°). The four main knots correspond to the northern end of the condensation A, the two [S II] peaks in the condensation B and the southern part of the lobe connecting B and C, respectively. The radial velocity increases from GGD 34/B to GGD 34/C, as observed in the spectrum taken with PA = 79°. However, the position-velocity diagrams inside the condensation GGD 34/B show slight differences between the two orientations. The [S II] lines split into two components in the maximum of the condensation B. The most intense shows a very rapid increase in the velocity as observed in Fig. 3 (PA ≃ 79°). The second, weaker component decreases in speed to the west. As before, condensation A only produces a faint continuum, strong Hα emission centered at 0 velocity, and perhaps some blueshifted [S II] emission.

The spectrum obtained with PA ≃ 162° only contains information about GGD 34/B. The condensation is barely resolved. Intense [S II], Hα and [N II] lines are detected. The [S II] lines are asymmetric and have a faint tail to large blueshifts.

Figure 5 displays the spectrum of the two maxima detected in the condensation A, PA = 20° (see Sect. 2.1). The region around the *I* peak in GGD 34/A (see Fig. 1), only produces Hα emission and the faint continuum observed in all the other spectra (see Figs. 3 and 4). The [S II] maximum, 2″.5 appart, has a completely different spectrum: strong [S II], [N II] and Hα lines are detected. All the lines are blueshifted around 200 km s^{-1}. The spatial extent of the line emitting region is very small (point like along the bow for the spatial resolution of our spectrograph). The [S II] lines are asymmetric with a wing to the red.

Therefore, the spectra show that the condensation GGD 34/A has two very different regions:

(i) An extended, bow-shaped region, characterized by a strong continuum and broad (FWHM ∼ 4.2 Å = 190 km s^{-1}) Hα emission centered at 0 velocity respect to the cloud. We denominate it: broad emission line region (BELR).

(ii) A small, arrow-shaped region, where the spectrum is dominated by the [S II], [N II] and Hα emission lines blueshifted ∼ 200 km s^{-1}. No continuum emission is detected. The emission lines are narrower: FWHM(Hα) ≃ 2.5 Å = 114 km s^{-1}. We denominate it: narrow emission line region (NELR).

3. Analysis of the spectra

3.1. Excitation and electronic densities

To estimate the excitation and electronic densities along GGD 34, we have extracted the individual spectrum of each knot as defined in Figs. 3, 4 and 5. The spectra have been obtained averaging three scan lines around the peak of each knot (3 scan lines ≃ 1″.9; seeing 2″). Radial velocities, electronic densities and excitations (ratios I(Hα)/I([S II]) and I([N II])/I([S II])) are given in Table 1. The

Table 1. Physical properties of GGD 34 inferred from the spectra

PA	Cond.	V_r(Hα)	V_r([S II]$_{6716}$)	V_r([S II]$_{6731}$)	V_r([N II]$_{6584}$)	V_r([S II]$_{6548}$)	N_e	Hα/[S II]	[N II]/[S II]
(°)		(km s^{-1})	(km s^{-1})	(km s^{-1})	(km s^{-1})	(km s^{-1})	(cm^{-3})		
79	a2	0							
	b1	−167	−147	−145	−141	−152	<1 10^2	0.65	0.16
	c1	−188	−186	−176	−201		<1 10^2	0.63	0.26
	c2	−152	−159	−160	−171		<1 10^2	0.65	0.16
108	a1	0							
	b2	−251	−284	−287			<1 10^2	0.96	
		−143	−128	−127	−130	−135	1.3 10^2	0.58	0.40
	b1	−186	−159	−162	−157	−167	<1 10^2	0.84	0.46
	c3	−190	−183	−189	−216		<1 10^2	0.47	0.26
162	b2		−275	−295			<1 10^2		
		−152	−131	−136	−145	−149	<1 10^2	0.73	0.39
20	a2	0							
		−200	−200	−196	−207		1.1 10^3	0.56	0.37

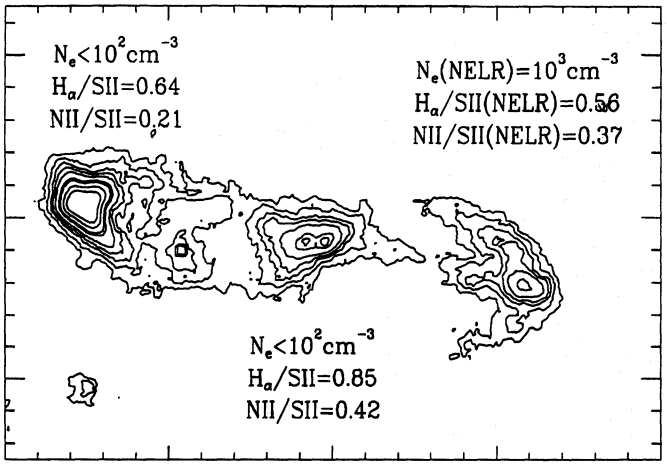

Fig. 6. Summary of the observed Ne and excitation conditions in the jet

spectrum of the condensation B, knot "b2", (PA: 108° and 162°; see Fig. 4) have two components that have been deblended into two gaussians to determine their physical parameters. The results are summarized in Fig. 6.

The electronic densities, N_e, have been estimated using the $[S\,II]_{6716/6730}$ diagnostic curve from Aller (1984), and assuming a fiducial temperature of 10^4 K. The electronic density is very low in the condensations C and B, $N_e \leqq 1.2\ 10^2\,cm^{-3}$, and it is even lower in the lobe. In the condensation GGD 34/A, the electronic density is an order of magnitude larger $N_e = 1.1\ 10^3\,cm^{-3}$.

The excitation is low and quite uniform in the flow. The Hα and [N II] strength relative to [S II] increases slightly from GGD 34/A to GGD 34/B and then decreases toward GGD 34/C. The values of the ratios agree with what is expected for very low velocity shocks. The grid of models for radiative shocks computed by Hartigan et al. (1987), indicates that for both bow-shocks and planar shocks models, these ratios are only accomplished by shocks with velocities $V_s \leqq 40\,km\,s^{-1}$. Typical theoretical values for $N_e = 1\ 10^2\,cm^{-3}$ and $V_s = 40\,km\,s^{-1}$ are Hα/[S II] = 3.2 and [N II]/[S II] = 0.6 (planar shock). These ratios decrease with the shock speed. Note that the models generate more Hα emission (or less [N II]) than observed. The *mean radial velocity* inferred from the blueshift of the lines is $\sim -180\,km\,s^{-1}$. This implies that the observed excitation has to be produced by oblique shocks even in the bright [S II] knot inside GGD 34/A.

The very low excitation of the object also indicates rather small ionization fractions, so that the electronic densities determined from the [S II] lines can be considerably smaller than the particle densities in the gas.

The electronic density has been also estimated for the NELR component of GGD 34/A. The value is an order of magnitude larger than in the rest of GGD 34, however the excitation conditions do not seem to vary much. This implies that the particle density in the NELR is probably of an order of magnitude larger than in the rest of GGD 34 since the excitation is approximately constant along GGD 34 and henceforth, the same ionization fraction is expected.

3.2. *Velocity field: position-velocity diagrams*

Individual spectra have been extracted along the object from the PA = 79° and 108° data. The velocity of each emission line has been determined by gaussian fitting, which is a good first order

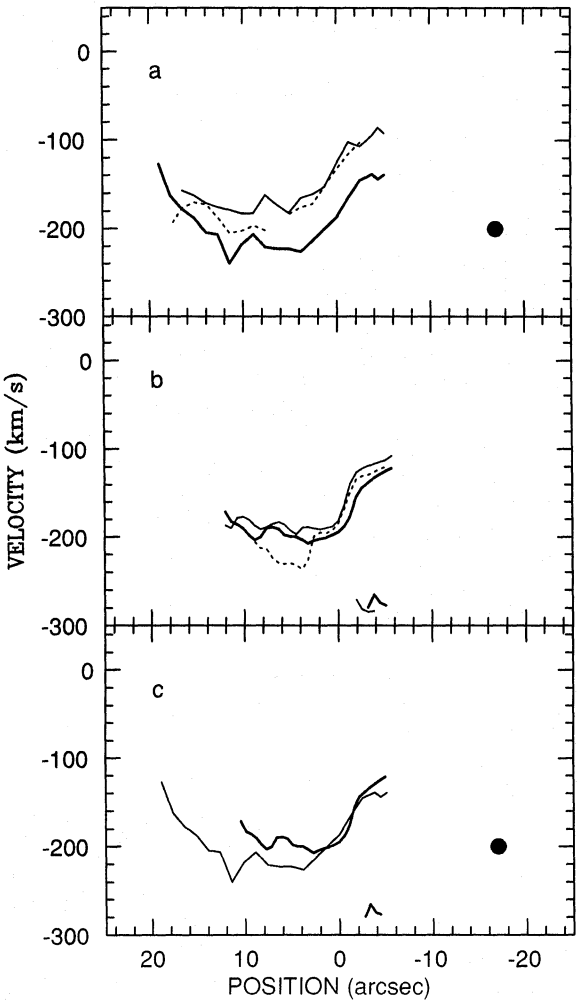

Fig. 7a–c. Velocity field of the jet. The velocity centroids of the different species are compared in **a** and **b** for slit orientations PA = 79° and PA = 108° respectively. The velocity of the [S II], [N II] and Hα lines is represented in both panels by a thin, a dotted and a thick line, respectively. In **c**, the Hα velocity field in the direction PA = 108° (thin line) is projected over PA = 79° (thick line)

approach in view of the shape of the line profiles. In the cases where two lines were clearly blended (e.g. PA = 108°), they have been deblended also assuming that both are gaussian. The results are shown in Fig. 7a and b for PA = 79° and 108°, respectively.

The overall aspect of the velocity field along the jet (PA = 79°) is sinusoidal. The velocity decreases very rapidly along B and then increases smoothly towards C. This impression is enhanced by the big filled circle that indicates the velocity of the jet at GGD 34/A (NELR). There are slight differences between [N II], [S II] and Hα. For instance, there is a more pronounced increase of the velocity along Hα in C than in the other lines, and also the mean velocity of Hα along the condensation B is larger than in the rest of the lines.

The spectrum along the major axis of the condensation GGD 34/B (PA = 108°) is quite similar except for a secondary velocity component along condensation B. In the peak of condensation B (PA = 108°), the flow is splitted into two components: the most intense shows a strong decrease in velocity eastwards and follows the pattern already described for PA = 79° (Fig. 7a); the faintest component is moving at much larger speeds. The velocity centroid of the two components is at $\simeq -200\,km\,s^{-1}$, which is the mean

velocity, previous to the splitting. [N II] velocity is significantly larger than [S II] and Hα in the central region and the velocity gradient points towards the high velocity component observed in these two lines. Inside the condensation B, the high velocity [N II] dissappears and only a low velocity component is observed. This is probably due to the weakness of the [N II] compared with the [S II] or Hα. In fact, a small bluewing starts to develop in the [N II] line after the passage of the flow by the peak of the condensation B.

An interesting feature is the stratification of the lines with the velocity (Fig. 7). [S II] lines have typically smaller velocities than Hα in the low velocity component and higher in the high velocity, defining the outer envelope of the velocity field. Small errors in the wavelength callibration cannot easily explain this systematic trend. Slightly different velocities could trace different locations across the cooling region transversal to the flow. In fact, our images (see Fig. 1) already indicate that the opening angle of the condensation B is larger (55°) in Hα than in [S II] (40°). Theoretical models of low velocity ($V = 40\,\mathrm{km\,s^{-1}}$) shocks predict sizes for the cooling region $\simeq 0.7$–350 AU, and a structure of the cooling region, in which Hα emission is produced very close to the shock front, followed by [S II] (Raga & Binette 1991). This is similar to the stratification suggested by our kinematical data.

Finally, we have projected the Hα velocity field in the direction PA = 108° over the PA = 79° (see Fig. 7c) multiplying by a factor cos(29°) the spatial coordinates. There are some differences, as expected from the morphology of GGD 34. The most noticeable is the larger velocity gradient of GGD 34/B when observed along the axis of symmetry of the condensation.

4. The nature of GGD 34

The morphology and the excitation conditions derived in Sect. 3.1 clearly indicate that GGD 34 is a collimated flow of gas illuminated by radiation generated in oblique shocks and therefore, GGD 34 is a jet.

The source exciting the jet seems to be located at the westernmost end of GGD 34/A. The broad Hα emission and the continuum coming from the BLER cannot be produced by the reflection of the jet radiation in a denser medium. Since the Hα line profile is similar to that observed in the pre-main-sequence (PMS) stars, the most suitable interpretation is that both, lines and continuum, are radiation coming from a PMS star that it is reflected at the borders of the cavity. The morphology of GGD 34/A also agrees with this interpretation. The intensity of the continuum and Hα decreases from the position "a 2" at the head of GGD 34/A towards "a 1" at the northeast end of the bow (see Fig. 1) suggesting that the illuminating source is very close to the center of the bow. This is also confirmed by the proper motions of the condensations towards the east (Ray et al. 1990).

Therefore, GGD 34 seems to be a jet departing from a YSO embedded in GGD 34/A that propagates towards GGD 34/B. GGD 34/B apparently representing a region where the flow shocks, frees energy and opens up to converge again in GGD 34/C. The width of the emission lobe varies between GGD 34/B and GGD 34/C by as much as a factor 3 at 3σ level (see Sect. 2.1) and, the maximum width of the jet, is as large as 1/5 of the jet length!. This makes GGD 34 a very peculiar jet.

These peculiar characteristics of GGD 34 can be best spelled out by a direct comparison with a "prototypical" jet, such as HH 34. HH 34 shows a chain of 12 well aligned knots that defines a highly collimated jet. The jet extends along 26″ ($\simeq 0.06$ pc) and the mean separation between knots is 500–1000 AU (Reipurth et al. 1986; Buhrke et al. 1988). It has been proposed that these radiating knots are generated in the crossing shocks that collimate the flow (Raga et al. 1990). The distance between two knots represents essentially a crossing shock. The comparison with GGD 34 shows three main differences:

(1) The size of a "crossing shock" in GGD 34 (interpreted as the distance between B and C) is an order of magnitude larger than that observed in the typical YSOs jets ($2\,10^4$ AU rather than $1\,10^3$ AU).

(2) The size of the "crossing shock" in GGD 34 is comparable to the "jet" length (one half), and not much smaller.

(3) GGD 34 is not symmetric with respect to the axis of the flow. In fact, the object has an helical or sinusoidal shape (symmetric with respect to the maximum of the condensation B).

The most striking property of GGD 34 is the *lack of significant variations in the excitation of the gas while the radial velocity of the flow changes by as much as 100 km s^{-1}*. This points out that the velocity variations of the jet do not play a major role in the excitation of the material.

5. Discussion

The velocity field of the GGD 34 between B and C is correlated with the variation of the morphology of the outflow. The [S II] and Hα images show that the emission lobe connecting GGD 34/B and C opens up between the two condensations. At the same time, the velocity of the gas increases from B to the east, decreasing again in C to the initial value in the peak of the condensation B (compare Figs. 1 and 7a). The velocity in the west end of B is $-120\,\mathrm{km\,s^{-1}}$, increases to $-200\,\mathrm{km\,s^{-1}}$ in between B and C and decreases again to $\simeq 120\,\mathrm{km\,s^{-1}}$ at the end of C. The velocity jump in GGD 34/B is suggestive of a shock jump (see Fig. 7b). However, a shock like this would heat the gas to temperatures of $\sim 3.8\,10^6$ K! Note that a jet with this temperature would expand with an opening angle of $\simeq 175°$ and would show extremely highly ionized species, not the low excitation lines that we observe. Note also that the excitation in the GGD 34 condensations is not much larger than in the intercondensation area. Therefore, the properties of GGD 34 in the region between GGD 34/B and GGD 34/C cannot be explained by a purely hydrodynamical jet excited and collimated by oblique shocks.

5.1. Pressure gradients in the external medium

The disturbed medium around GGD 34 could be bending the jet. In fact, there is a very steep gradient in the cloud turbulence around GGD 34. The FWHM of the ^{12}CO emission varies from $2.9\,\mathrm{km\,s^{-1}}$ in the north-east of GGD 34 to $4.4\,\mathrm{km\,s^{-1}}$ in the south-west (Fig. 5, Bechis et al. 1978). These line widths are highly suprathermal since the kinetic temperature of the gas inferred from the CO is $\leqq 30$ K (Bechis et al. 1978). So the pressure experienced by the jet from the external medium could be bending it significantly in the SW–NE direction. However, the distortion of GGD 34 between B and C points towards the South, which is the more pressurized area according to the radio maps. Therefore, the external medium does not seem to be acting in this simple way.

5.2. Jet instability

The correlation between the velocity field and the morphology suggests that the variations in speed are due to geometric projection effects. This, in turn, would imply that the jet itself has a

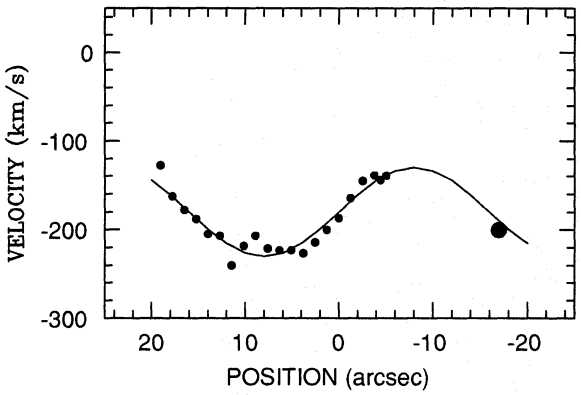

Fig. 8. The best fit to the radial velocity field of GGD 34 is illustrated (thin line) on top of the observed one (thick line) (see text)

quite sinusoidal shape. All these data, and especially the symmetries inferred from them could be explained if there was a helical plasma instability acting over GGD 34. The are two major instabilities that can produce the sinusoidal distortions of GGD 34: magnetic "kink" instabilities and Kelvin-Hemholtz instabilities. The first are induced by the conservation of the magnetic flux along the jet, while the K–H instabilities are due to boundary effects between the jet and the external medium.

The kink mode of a K–H instability would distort the jet to a sine curve and, therefore the velocity field. In fact, the GGD 34 velocity field can be fitted reasonably well to a cosine function modulating the perturbation over a constant projected jet speed of $-180\,\mathrm{km\,s^{-1}}$ (see Fig. 8). The best fit is,

$$V_r = [-50 \times \cos\left(\frac{2\pi x}{32''}\right) - 180]\,\mathrm{km\,s^{-1}}$$

Note that if we extrapolate the curve towards condensation A, the velocity of the flow expected there is $\simeq -200\,\mathrm{km\,s^{-1}}$. This is the speed of the [S II], [N II] and Hα lines in the NELR of GGD 34/A (see also Table 1).

Therefore, we suggest that the peculiar properties of GGD 34 are produced by the action of a "kink" plasma instability.

5.3. *Jet from variable a source?*

Variations in the ejection direction can produce peculiar morphologies in jets. A recent analysis of the problem in the case of ballistic jets (high Mach number, high density jet) by Raga et al. (1992) shows that initially small side-to-side oscillations in the jet are amplified further downstream. For instance, a flow coming from a precessing source results in a "helical" jet moving around a conical surface (see Figs. 3 and 4 in Raga et al. 1992). There are, however, several problems with this interpretation in the case of GGD 34. First of all, note that GGD 34/B and C are connected by an emission lobe that extends asymmetrically to *both sides of the jet axis* and therefore its morphology cannot be described by a helix around a conical surface. Moreover, there is a clear opening and focusing of the jet between GGD 34/B and C that cannot be easily explained in this scenario. If the internal pressure of the jet is high enough, the jet could be opening up as it describes the helical pattern, however it looks difficult to focus it back in GGD 34/C by pure hydrodynamical means (see above).

6. Conclusions

GGD 34 is a peculiar jet that shows large distortions from linearity correlated with large variations in the velocity field by as much as $100\,\mathrm{km\,s^{-1}}$. These distortions are not accompanied by significant changes in gas density and temperature, which makes it very difficult to explain it as a standard hydrodynamical jet collimated by oblique shocks.

The correlation between morphology and velocity field can be then explained by geometric projection effects. This implies that the jet is physically curled and that the gas is moving along this surface. This kind of distortions is expected in plasma beams undergoing a major instability. We believe that the peculiar physical characteristics of GGD 34 can be explained if a "kink" plasma instability is acting over the jet and giving it its sinusoidal shape.

Acknowledgements. Ana I. Gómez de Castro thanks Alejandro Raga for many insightful conversations about jet hydrodynamics. We also thank the staff at the Calar Alto Observatory for their assistence during the observations. Ana I. Gómez de Castro is grateful to the Ministery of Education of Spain for a "Beca de Reicorporación". This work has been supported in part by PB87-0187.

References

Aller L.H., 1984, Physics of Thermal Gaseous Nebulae. Reidel, Dordrecht, p. 138
Bechis K.P., Harvey P.M., Campbell M.F., Hoffmann W.F., 1978, ApJ 226, 439
Buhrke T., Mundt R., Ray T.P., 1988, A&A 200, 99
Eiroa C., Gómez de Castro A.I., Miranda L.F., 1992, A&AS 92, 721
Gómez de Castro A.I., 1989, Ph. D. Thesis Universidad Complutense de Madrid
Hartigan P., Lada C.J., 1985, ApJS 58, 383
Hartigan P., Raymond J., Hartmann L., 1987, ApJ 316, 323
Mundt R., Brugel E.W., Buhrke T., 1987, ApJ 319, 275
Racine R., 1968, AJ 73, 233
Raga A., Binette L., Cantó J., 1990, ApJ 360, 612
Rage A., Binette L., 1991, Rev. Mex. Astron. 22, 265
Raga A., Cantó J., Biro S., 1992 (in press)
Ray T.P., 1987, A&A 171, 145
Ray T.P., Poetzel R., Solf J., Mundt R., 1990, ApJ 357, L45
Reipurth B., Bally J., Graham J.A., Lane A.P., Zealey W.J., 1986, A&A 164, 51
Reipurth B., 1989, Proc. of the ESO Workshop on Low Mass Star Formation and Pre-Main Sequence Objects, Reipurth B. (ed.) ESO, Garching bei München, p. 247
Reipurth B., Heathcote S., 1991, A&A 246, 511